

Origin of the long-range ferrimagnetic ordering in cubic $\text{Mn}(\text{Co})\text{Cr}_2\text{O}_4$ spinels

Abhishek Das,¹ Pratap Pal,^{1,2} Dheeraj Ranaut,³ Kazi Parvez Islam,¹ Gourab Bhattacharya,⁴ Sakshi Mehta,⁵ Abhishake Mondal,⁵ Venimadhav Adyam,⁴ K. Mukherjee,³ Amitabh Das,^{6,7} and Debraj Choudhury^{1,*}

¹Department of Physics, Indian Institute of Technology Kharagpur, West Bengal 721302, India

²Department of Materials Science and Engineering, University of Wisconsin, Madison, Wisconsin 53706, USA


³School of Physical Sciences, Indian Institute of Technology Mandi, Mandi 175075, Himachal Pradesh, India

⁴Cryogenic Engineering Centre, Indian Institute of Technology Kharagpur, West Bengal 721302, India

⁵Solid State and Structural Chemistry Unit, Indian Institute of Science Bengaluru, Karnataka 560012, India

⁶Solid State Physics Division, Bhabha Atomic Research Centre Mumbai, Mumbai 400 085, India

⁷Department of Physical Sciences, Homi Bhabha National Institute, Mumbai 400094, India

 (Received 25 November 2022; revised 10 February 2023; accepted 10 March 2023; published 20 March 2023)

Structural transition from a cubic to a tetragonal phase in magnetically frustrated AB_2O_4 spinel compounds is generally found indispensable to enable long-range magnetic ordering. Intriguingly, MnCr_2O_4 and CoCr_2O_4 , constitute exceptions to the above general rule, as they seem to undergo long-range ferrimagnetic (FIM) ordering without any structural involvement in their corresponding cubic phases. We find that MnCr_2O_4 (and CoCr_2O_4) undergo a hitherto undetected partial glassy magnetic ordering of the spiral-spin components at a temperature (T_{SP}) higher than the long-range FIM transition. The spin-glass transition at T_{SP} triggers the onset of structural modifications that helps to reduce the geometric-magnetic-frustration and thereby enable the long-range FIM ordering within an overall cubic phase. In the absence of the higher-temperature glassy transition in doped MnCr_2O_4 , the corresponding magnetic ordering is found to be glassy instead of being a long-ranged FIM ordering. In magnetic spinel oxides, like CdCr_2O_4 and FeCr_2O_4 , where cubic to tetragonal structural transition occurs from either a spin-Jahn-Teller effect or through Jahn-Teller distortions, such a higher-temperature glassy magnetic transition (i.e., above the long-range magnetic ordering) is absent. Our results, thus, clearly elucidate that the structural modifications associated with the glassy magnetic ordering at T_{SP} , aided with presence of magnetic A -site ions, play a pivotal role in releasing the geometric-magnetic-frustration in MnCr_2O_4 (and also CoCr_2O_4) to enable long-range FIM ordering in these systems.

DOI: [10.1103/PhysRevB.107.L100414](https://doi.org/10.1103/PhysRevB.107.L100414)

The phenomenon of geometric magnetic frustration (GMF) in a crystalline solid refers to the inability of any magnetically ordered state to simultaneously satisfy various competing exchange interactions, arising from the geometry of the underlying lattice [1,2], as seen in Sec. I of Supplemental Material [3]. The GMF phenomenon causes large degeneracies for the ground state and an inability for even dense magnetic systems to undergo long-range magnetic ordering down to the lowest temperature [4,5]. Cubic AB_2O_4 spinel oxides [the representative structure is shown in Fig. 1(a)], where the magnetic B sites lie on a frustrated pyrochlore lattice, as shown in Fig. 1(a), host strong GMF. In the presence of strong spin-phonon coupling, AB_2O_4 spinel oxides often undergo a structural transition that helps to reduce the GMF [6] and enable the realization of novel magnetic ground states [7–9]. The decisive role of structural degrees of freedom towards long-range magnetic/ferroelectric ordering in other family of GMF oxides have also been stressed [10–14].

The structural transition in cubic AB_2O_4 spinel oxides is often driven by Jahn-Teller (JT) distortions from the presence of either JT active A -site ions [as in ACr_2O_4 , $A = \text{Fe}^{2+}(3d^6)$,

$\text{Ni}^{2+}(3d^8)$, $\text{Cu}^{2+}(3d^9)$ [15–17], where B -site $\text{Cr}^{3+}(3d^3)$ ion is JT inactive, represented in Fig. 1(d) and 1(f)] or from JT active B -site ions [as in CdV_2O_4 [18], MnTi_2O_4 [19,20] comprising of JT active $\text{V}^{3+}(3d^2)$ and $\text{Ti}^{3+}(3d^1)$ ions, respectively]. The structural transition can also arise from a purely spin-driven mechanism stemming from strong spin-lattice coupling (as in ACr_2O_4 , $A = \text{Mg}, \text{Cd}, \text{Zn}$, which include nonmagnetic, JT inactive A -site ions [21–24]), which is referred to as the spin-JT effect.

Surprisingly, MnCr_2O_4 and CoCr_2O_4 , which in addition to magnetic B -site ions, contain magnetic (and JT-inactive) A -site ions, as represented in Figs. 1(c) and 1(e), were found to undergo long-range magnetic ordering without involvement of any structural changes [25,26]. The presence of magnetic ions at both A and B sites introduces additional AA and AB exchange interactions in AB_2O_4 spinels that can reduce the GMF. As a representative example for this pair, we will focus on MnCr_2O_4 in the manuscript. MnCr_2O_4 is reported to undergo a collinear long-range ferrimagnetic transition at T_{N1} followed by a re-entrant glass transition into a modified Lyons-Kaplan-Dwight-Menyuk [27–30] ferrimagnetic spiral at a further lower temperature T_{N2} . Interestingly, the longitudinal and the transverse spin components of the ferrimagnetic spiral of MnCr_2O_4 exhibit different qualitative

*debraj@phy.iitkgp.ac.in

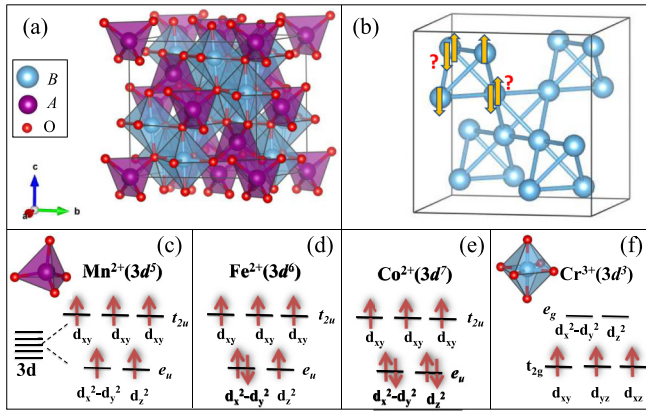


FIG. 1. (a) Room-temperature cubic crystal structure of AB_2O_4 spinels, where A and B ions are within tetrahedral and octahedral oxygen environments, respectively. (b) illustrates the pyrochlore network (corner shared tetrahedra) of the magnetic B -site ions and a schematic representation of the associated magnetic frustration. Schematic electronic configurations for the tetrahedrally coordinated (c) Mn^{2+} ($3d^5$), (d) Fe^{2+} ($3d^6$), (e) Co^{2+} ($3d^7$) and octahedrally coordinated (f) Cr^{3+} ($3d^3$) ions.

features. Long-range order was detected for the longitudinal spin components, whereas the transverse (or spiral) spin component exhibits short-range glassy order below T_{N2} [31]. Short-range magnetic correlation among the transverse (spiral) spin components, interestingly, is found to exist till much above T_{N2} and T_{N1} [31,32]. The presence of glassy order for the spiral-spin component clearly brings out the insufficiency of the magnetic A -site ion to fully release the GMF effect and suggests an alternative or supporting mechanism that leads to the long-range ferrimagnetic ordering in $MnCr_2O_4$. In this letter, we report the presence of a partial (weak) glassy ordering of the spiral-spin components at T_{SP} , which is ~ 6 K above T_{N1} , and a more complete order for the spiral components to occur at T_{N2} . Importantly, the spin-glass order at T_{SP} is associated with the onset of structural changes, manifested through a change in slope of the temperature dependence of Cr-Cr distance and sharp changes in the oxygen-ion positions, Mn-O and Cr-O bond distances, and Cr-O-Cr and Mn-O-Cr angles at T_{SP} . Such structural changes within the overall cubic structure help to circumvent the GMF, already weakened by the presence of magnetic A -site ions (as explained above), and lead to long-range ferrimagnetic ordering at T_{N1} in $MnCr_2O_4$. An absence of the higher-temperature glassy transition, in adequately doped $MnCr_2O_4$, causes the ferrimagnetic transition at T_{N1} to be glassy instead of being long-ranged, thereby, revealing its critical role towards the stabilization of long-range ferrimagnetic ordering in this class of systems.

Phase-pure polycrystalline ACr_2O_4 ($A=Mn, Fe, Co$ and Cd) samples were prepared via solid state synthesis; well ground stoichiometric mixtures of Cr_2O_3 and MnO (for $A=Mn$), Fe_2O_3 and Fe powder (for $A=Fe$), CoO (for $A=Co$), CdO for ($A=Cd$) were sintered inside evacuated quartz tubes at $1150^\circ C$ for 24 h. $Mn_{0.60}Cd_{0.13}Zn_{0.27}Cr_2O_4$ (possessing similar Cr lattice as $MnCr_2O_4$) and $MnCr_2O_4$ -Q (which was additionally quenched into liquid N_2 directly from $1150^\circ C$) were also prepared using similar synthesis conditions to act

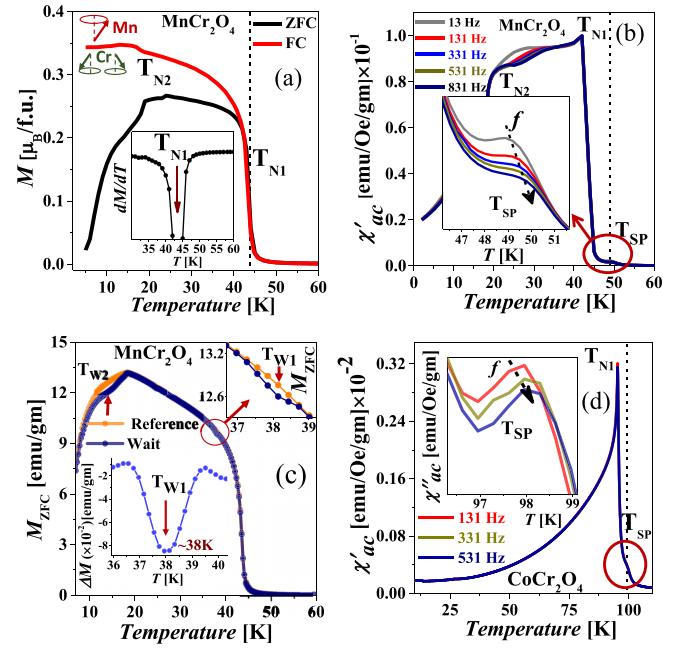


FIG. 2. (a) $M(T)$ curves of $MnCr_2O_4$ measured at $H=100$ Oe. Inset depicts the dM/dT vs T plot. Schematic of FIM spiral configurations involving Cr and Mn spins are shown in the top left corner, where the dashed line represents the direction of the longitudinal spin component. (b) The real part $\chi'(T)$ of ac susceptibility data of $MnCr_2O_4$. The inset shows the enlarged view around the spin-glass transition at T_{SP} . (c) Results of dc memory experiments for $MnCr_2O_4$, where the insets exhibit clear aging and memory effects below T_{N2} and also between T_{N1} and T_{N2} . (d) $\chi''(T)$ data of $CoCr_2O_4$ with different frequencies. The inset highlights the imaginary part $\chi''(T)$ of the ac susceptibility data of $CoCr_2O_4$ around T_{SP} .

as reference compounds. Room-temperature x-ray diffraction (XRD) measurements using $Cu K\alpha$ source elucidate that all the synthesized spinel-oxides crystallize in the cubic $Fd-3m$ structure at room-temperature (full spectra and Rietveld refinement of a representative sample $MnCr_2O_4$ are shown in Figs. S2(a) and S2(b), respectively, of Ref. [3]), with trace amounts ($\sim 1\%$) of Cr_2O_3 impurity phase. Temperature-dependent neutron diffraction (for $\lambda \approx 1.2443$ Å) experiments were performed at Dhruva reactor, Bhabha Atomic Research Centre, Mumbai, India to probe magnetic order and structural changes. Temperature-dependent ac- (over a dc-magnetic field of 1 Oe) and dc-magnetic measurements were carried out using magnetic property measurement system (MPMS) from quantum design. Magnetic dc memory experiments were performed by measuring dc zero-field-cooled (ZFC) magnetization (M) data with and without an intermediate wait at a specific temperature of interest (T_W) and then investigating the difference (ΔM) of these recorded ZFC data. The temperature-dependent dc-magnetization data [Fig. 2(a)] indicate that $MnCr_2O_4$ undergoes a paramagnetic to ferrimagnetic transition at T_{N1} , which is followed by a glass transition at T_{N2} , as reported earlier [31]. Interestingly, ac-magnetic susceptibility measurement, which is a very sensitive technique to probe weak magnetic transitions [33,34], detect the presence of an additional (hitherto undetected) weak magnetic

transition at T_{SP} just above the ferrimagnetic (FIM) ordering ($T_{N1}=43$ K), as shown in Fig. 2(b). Importantly, the magnetic transition at T_{SP} is not discernible even in the temperature-derivative of the dc-magnetic data [as seen in the inset of Fig. 2(a)], presumably due to associated large background magnetic signal. A similar magnetic transition at $T_{SP} \sim 98$ K is also detected above the ferrimagnetic transition of $T_{N1}=95$ K in CoCr_2O_4 (corresponding dc-magnetization data and imaginary part (χ'') of the ac susceptibility data are shown in Figs. S3(a) and S3(b), respectively of Ref. [3]) using ac-susceptibility measurements, as shown in Fig. 2(d), bringing out the intrinsic nature of this transition in these two systems. Notably, the Cr_2O_3 impurity phase ($\sim 1\%$) does not exhibit any magnetic transition in this entire temperature window [35]. The magnetic transition at T_{SP} (and also T_{N2}) is found to be glassy since the corresponding peak position (T_f) strongly disperses with frequency (f) of the ac-magnetic field as seen in the insets of Figs. 2(b) and 2(d) (the frequency dispersive nature of the transition at T_{N2} for CoCr_2O_4 is clearly discernible in the corresponding χ'' data, as shown in Fig. S3(b) of Ref. [3]). A critical slowing-down analysis (using a power law model [36]) is employed to investigate the nature of the glassy magnetic transition associated with T_{SP} (the detailed analysis is discussed in Sec. IV of Ref. [3]). The extracted τ_0 ($\sim 1 \times 10^{-13}$ sec) and $z\nu$ values (~ 6.4) from the best fit to the power law model, as shown in Fig. S4(a) of Ref. [3] for MnCr_2O_4 , are typical to spin-glass systems [37–39], thereby, elucidating that MnCr_2O_4 (and also CoCr_2O_4) undergoes a spin-glass transition at T_{SP} prior to undergoing long-range FIM ordering at T_{N1} . The long-range nature of the magnetic transition at T_{N1} is established since χ' and χ'' peak positions associated with T_{N1} do not disperse with varying f , as seen in Figs. 2(b) and 2(d). In order to investigate the presence of aging and memory effects, dc memory experiments were performed on MnCr_2O_4 with two intermediate waits at T_{W1} (between T_{N1} and T_{N2}) and at T_{W2} (below T_{N2}). Presence of a dip in ΔM (the difference ZFC data, as discussed earlier) at the waiting temperature is a characteristic signature of a magnetic glass system [40]. Distinct dips in ΔM were clearly observed at both the wait temperatures, T_{W1} [as seen in the inset of Fig. 2(c)] and T_{W2} . While the presence of aging and memory effects at temperatures below T_{N2} (which is a glass transition temperature) is expected, its presence between T_{N2} and T_{N1} (which cannot be explained by the mere presence of a long-range magnetic ordering at T_{N1}) suggests that part of the magnetic component that develops spin-glass-like dynamics below T_{SP} do not undergo long-range magnetic ordering at T_{N1} . The τ_0 and $z\nu$ values, determined from the best fits to the relaxations observed at T_{N2} , as shown in Fig. S4(b) (for MnCr_2O_4) and (d) (for CoCr_2O_4) of Ref. [3], indicate T_{N2} to be cluster-glass transition [38,39]. The slower cluster-glass dynamics likely arises due to spins at the interface between ferrimagnetic domains with different short-range orders, as determined in Ref. [31].

In the following, we discuss the magnetic order as probed by neutrons. The temperature dependences of the intensity of various neutron diffraction peaks is shown as a contour plot in Fig. S5(a) of Ref. [3]. In the $Fd-3$ space group of MnCr_2O_4 , Mn occupies $(\frac{1}{8}, \frac{1}{8}, \frac{1}{8})$, Cr $(\frac{1}{2}, \frac{1}{2}, \frac{1}{2})$, and O (x, x, x) positions.

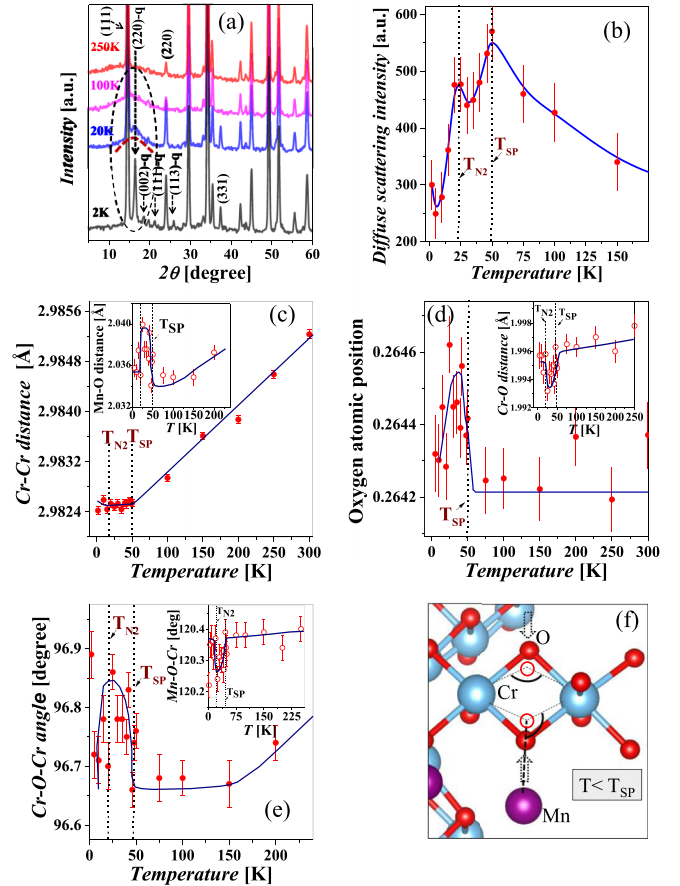


FIG. 3. (a) Neutron diffraction patterns of MnCr_2O_4 at selected temperatures. The brick-red thick dashed line immediately below the 18 K spectrum below the (220)-q peak highlights the corresponding diffuse scattering intensity. (b) Variation of diffuse scattering peak intensity with temperature. (c) Variation of Cr-Cr distance (d) oxygen position and (e) Cr-O-Cr angle with temperature. The insets to (c), (d), and (e) highlight the anomalous changes in Mn-O bond distance, Cr-O bond distance and Mn-O-Cr angle below T_{SP} , respectively. The blue solid line running through the data in (b), (c), (d), and (e) are corresponding guides to the eye. (f) Schematic representation of the structural modifications within the cubic phase below T_{SP} . The open red circles refer to the new oxygen positions below T_{SP} .

On lowering of temperature below 42 K (T_{N1}), enhancement in the intensity of the fundamental reflections (111), (220) and (331) is observed, as seen in Figs. 3(a) and S5(a) of Ref. [3], indicating the onset of magnetic ordering in the sample. The refined magnetic structure [the representative refined plots for 50, 30, and 2 K spectra are depicted in Figs. S5(c), S5(d), and S5(e) of Ref. [3], respectively] is observed to be collinear ferrimagnetic involving the moments on Mn^{2+} and Cr^{3+} , as shown in the Fig. S5(f) of Ref. [3]. On further lowering of temperature, below 20 K (T_{N2}), a relatively strong (220)-q and few weak (002)-q, (111)-q, (200)-q, and (113)-q superlattice reflections are observed (as shown in Figs. 3(a) and S5(a) of Ref. [3]). The temperature evolution of the intensity of the (220) fundamental and the (220)-q superlattice reflections are shown in Fig. S5(b) of Ref. [3]. The magnetic structure below T_{N2} was found to be a collinear ferrimagnetic structure coexisting with a noncollinear spiral structure described by

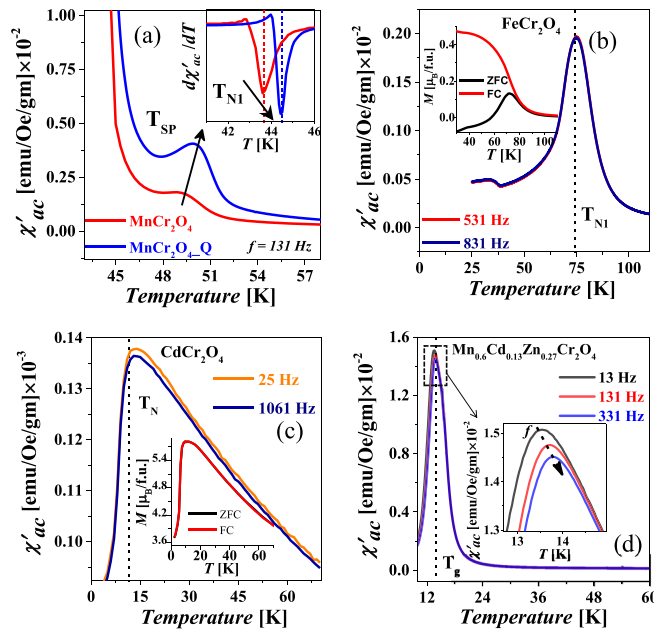


FIG. 4. (a) Comparative temperature (T) variations of the ac susceptibility data of MnCr_2O_4 and $\text{MnCr}_2\text{O}_4\text{-Q}$. The inset exhibits the enlarged view of the temperature-derivative of the χ' data around T_{N1} . χ' vs T plots of (b) FeCr_2O_4 , (c) CdCr_2O_4 , and (d) $\text{Mn}_{0.6}\text{Cd}_{0.13}\text{Zn}_{0.27}\text{Cr}_2\text{O}_4$. The insets in (b) and (c) highlight the corresponding dc-magnetization data. The inset in (d) highlights the enlarged view of the $\chi'(T)$ data around the magnetic ordering at 14K.

the propagation vector, $q = (0.622, 0.622, 0)$. Although the (220) - q satellite peak can be detected above T_{N2} in CoCr_2O_4 [31], the same does not apply in MnCr_2O_4 , presumably driven by the larger A -site spin moment ($5 \mu_B$ for Mn^{2+} as compared to $3 \mu_B$ for Co^{2+}) in the latter, that helps to decrease the GMF further and lead to weaker spin-glass dynamics of the spiral-spin components. The scenario of weaker GMF is also consistent with a relatively faster spin dynamics around T_{SP} in MnCr_2O_4 as compared to CoCr_2O_4 (as shown in Figs. S4(a) and (c) of Ref. [3]). Indeed, the χ' peak at T_{SP} becomes stronger [as seen in Fig. 4(a)] in specially synthesized disordered MnCr_2O_4 ($\text{MnCr}_2\text{O}_4\text{-Q}$), which is associated with some Mn-site vacancies which results in a weaker A -site overall magnetic moment. The Mn-site vacancies of $\text{MnCr}_2\text{O}_4\text{-Q}$ appear due to the presence of few Mn ions at the B - (Cr) site, which drives out an equal number of Cr atoms from the system and causes them to oxidize into the $\sim 5\%$ Cr_2O_3 impurity phase, as seen in the corresponding XRD spectrum in Fig. S6 and in related discussions in Sec. VI of Ref. [3]. The stronger and sharper χ' peak at T_{SP} in $\text{MnCr}_2\text{O}_4\text{-Q}$ is also associated with a concomitant increase in the temperature T_{N1} , as seen in the inset to Fig. 4(a), suggesting a positive correlation between the two phenomena. Interestingly, the suppression of spiral order above $T_{N2} \sim 20$ K is followed with a short-range magnetic ordering characterized by the presence of diffuse scattering centered at the (220) - q reflection extending to temperatures about $10T_{N2}$, as seen in Figs. 3(a) and S5(a) of Ref. [3]. Such a diffuse scattering is, however, not detected below the (220) neutron peak [as seen in Fig. 3(a)], ruling out the role of any atomic clustering in giving rise

to such diffuse scattering intensity. It is also observed that the presence of the diffuse scattering, evident from the hump around the (220) - q reflection, is not completely suppressed even at $0.1T_{N2}$, which indicates the presence of short-range magnetic correlations well into the magnetically ordered state. As seen in the temperature-dependent variation of the diffuse scattering intensity in Fig. 3(b), a small and broad decrease of the diffuse scattering intensity is observed first at T_{SP} followed by another sharp and larger decrease at T_{N2} . Similar decreases in the diffuse scattering intensity at the onset of spin-glass order have been found in related oxide systems [41,42]. It is significant that the weak decrease of diffuse peak intensity at T_{SP} , which is associated with a concomitant glassy ordering of the spiral spin components, occurs well above the long-range ferrimagnetic order at T_{N1} .

Since neutrons are sensitive to small structural changes, even those associated with movement of light oxygen atoms, temperature-dependent structural parameters, determined from refinement of neutron diffraction spectra with cubic $Fd-3m$ space group, were investigated to probe the origin of long-range magnetic order at T_{N1} . Clear magnetostructural anomalies are observed in the temperature dependences of the refined oxygen positions, Mn-O and Cr-O bond distances, Cr-O-Cr and Mn-O-Cr angles below T_{SP} , as seen in Figs. 3(d) and 3(e) and the corresponding insets of Figs. 3(c) to 3(e). The initial deviation of the oxygen position from the ideal position $(\frac{1}{8}, \frac{1}{8}, \frac{1}{8})$ of the fcc array, as seen at higher temperatures, is commonly known to arise in cubic spinel structure from ionic site mismatch [25,43,44]). The Cr-Cr bond distance (and also, the cubic lattice parameter, as shown in Fig. S7 of Ref. [3]) exhibits a normal linear thermal contraction with lowering of temperature above T_{SP} , however, it becomes nearly temperature-independent below T_{SP} . Importantly, the observed structural changes that emerge just below T_{SP} [schematically summarized in Fig. 3(f)] relate to a movement of the edge-shared oxygen ions in between the neighboring Cr ions, thereby, inhibiting the temperature-induced contraction in Cr-Cr bond distance with lowering of temperature below T_{SP} . Thus the anomalous flattening of the Cr-Cr distance below T_{SP} can be understood to arise from two opposite contributions, one associated with the normal contraction of the Cr-Cr distance (or lattice parameter) with lowering in temperature and another from an anomalous thermal expansion contribution (as observed in many spin-frustrated systems [45,46]), with the later contribution emerging only below T_{SP} . Since reduction in Cr-Cr bond distance causes an increase in the antiferromagnetic direct-exchange interaction, such an anomalous thermal expansion contribution, which relates to increase in Cr-Cr bond distance with lowering of temperature, leads to an effective reduction of GMF just below T_{SP} . In regards to the ferromagnetic Cr-O-Cr superexchange interaction, a decrease induced by an increase in Cr-O-Cr bond angle is likely balanced by a corresponding increase arising from a concomitant reduction in Cr-O bond distance below T_{SP} . First-principles calculations indeed suggest that Cr-Cr direct antiferromagnetic exchange dominates over Cr-O-Cr ferromagnetic superexchange interaction in MnCr_2O_4 [47]. Thus, the above magnetostructural changes below T_{SP} , along with presence of magnetic A -site ions, become critical to enable the long-range magnetic

ordering at T_{N1} . A consequent reversal in the trend of the magnetostructural changes below T_{N2} [as seen in Figs. 3(c)–3(e)] likely leads to the related low-temperature glass transition.

To understand whether presence of a glassy magnetic transition above the ferrimagnetic transition T_{N1} is a generic phenomenon in other chromate spinel oxides as well, we investigated representative members from two other broad classes of chromate-spinel oxides; one which undergoes a JT-distortion-driven structural transition at temperatures much above T_{N1} (similar to FeCr_2O_4) and another which undergoes a concomitant long-range magnetostructural transition due to the spin-JT effect (as in CdCr_2O_4). FeCr_2O_4 , driven by JT-active $\text{Fe}^{2+}(3d^6)$ ions, goes through successive symmetry-lowering structural transitions, one from cubic to tetragonal structure at $T_{S1} \sim 140$ K followed by tetragonal to orthorhombic structure at $T_{S2} \sim 75$ K, and the latter is associated with long-range ferrimagnetic ordering [48]. CdCr_2O_4 , which contains nonmagnetic A -site ($\text{Cd}^{2+}[4d^0]$) ions, also undergoes a spin-JT induced cubic to tetragonal structural transition accompanied with a concomitant long-range magnetic ordering [22]. Importantly, the higher-temperature glassy magnetic transition at T_{SP} (as observed in MnCr_2O_4 and CoCr_2O_4) is found to be absent in both FeCr_2O_4 and CdCr_2O_4 in their corresponding ac susceptibility data, as depicted in Figs. 4(b) and 4(c), respectively. Both these compounds do exhibit the presence of long-range magnetic ordering [corresponding dc magnetic data is shown in the insets of Figs. 4(b) and 4(c), respectively], characterized by a dispersionless χ' peak (see Fig. S8 of Ref. [3]). Clearly, thus, in the presence of a global structural transition, chromate spinel oxides directly undergo a long-range magnetic ordering and only in the absence of a global structural transition, does a higher-temperature glassy magnetic transition with accompanying weak structural changes become a necessary primer to reduce the GMF to enable long-range magnetic ordering. In the following, we have investigated a $\text{Mn}_{0.60}\text{Cd}_{0.13}\text{Zn}_{0.27}\text{Cr}_2\text{O}_4$ compound, which is carefully engineered to have nearly identical lattice parameters

(as indicated by Fig. S6 of Ref. [3]) and a Cr-Cr bond distance as in parent MnCr_2O_4 . Due to very different ionic radii of tetrahedrally coordinated $\text{Cd}^{2+}(0.78 \text{ \AA})$, $\text{Mn}^{2+}(0.66 \text{ \AA})$, and $\text{Zn}^{2+}(0.60 \text{ \AA})$ ions, $\text{Mn}_{0.60}\text{Cd}_{0.13}\text{Zn}_{0.27}\text{Cr}_2\text{O}_4$ is associated with significant A -site related size-disorder within an overall cubic structure, as shown in Fig. S2(a) of Ref. [3]. Interestingly, this helps us to realize a closely related compound to MnCr_2O_4 which do not undergo a higher-temperature glassy magnetic transition at T_{SP} , presumably due to the presence of random strain fields, and consequently, the associated ferrimagnetic transition at T_{N1} (reduced in temperature due to significant Mn-site spin dilution) become short-ranged (glassy), as seen in Fig. 4(d) and its inset. This further helps to shed light on the likely spin-JT related origin for the structural changes associated with T_{SP} .

In summary, through careful and detailed investigations on $A\text{Cr}_2\text{O}_4$ ($A = \text{Mn, Fe, Co}$ and Cd) spinel compounds, we identify the presence of a higher-temperature spin-glass ordering just above the long-range FIM ordering in MnCr_2O_4 and CoCr_2O_4 . Importantly, this high-temperature spin-glass ordering is associated with the nucleation of structural changes which enable significant reduction of the GMF. The presence of a magnetic A -site ion also helps to reduce the GMF effect associated with the pyrochlore B -lattice. These two effects, thus work together to enable long-range ferrimagnetic ordering in MnCr_2O_4 (and also CoCr_2O_4). Further theoretical investigations to probe the role of the observed structural changes towards enabling magnetic ordering in chromate spinel oxides will be helpful to understand and tune the associated functional properties.

A.D. acknowledges the financial support from MoE, India. D.C. acknowledges STARS, MoE (funding under Project file No. STARS/APR2019/NS/238/FS) and the INSA YS project for financial support. A.M. thanks the Solid State and Structural Chemistry Unit at the Indian Institute of Science (IISc) Bangalore, India, for providing the superconducting quantum interference device magnetometer facility.

-
- [1] L. Balents, *Nature (London)* **464**, 199 (2010).
 [2] A. P. Ramirez, *Annu. Rev. Mater. Sci.* **24**, 453-80 (1994).
 [3] See Supplemental Material at <http://link.aps.org/supplemental/10.1103/PhysRevB.107.L100414> for supporting structural and magnetization data. Rietveld-refined neutron diffraction data and analyses of ac-susceptibility relaxations with critical slowing down model are also included.
 [4] A. P. Ramirez, C. L. Broholm, R. J. Cava, and G. R. Kowach, *Phys. B* **280**, 290 (2000).
 [5] S. Kundu, A. Hossain, S. Pranava Keerthi, R. Das, M. Baenitz, P. J. Baker, J.-C. Orain, D. C. Joshi, R. Mathieu, P. Mahadevan, S. Pujari, S. Bhattacharjee, A. V. Mahajan, and D. D. Sarma, *Phys. Rev. Lett.* **125**, 117206 (2020).
 [6] V. Tsurkan, H.-A. Krug Von Nidda, J. Deisenhofer, P. Lunkenheimer, and A. Loidl, *Phys. Rep.* **926**, 1 (2021).
 [7] Y. Yamasaki, S. Miyasaka, Y. Kaneko, J.-P. He, T. Arima, and Y. Tokura, *Phys. Rev. Lett.* **96**, 207204 (2006).
 [8] K. Sing, A. Maignan, C. Simon, and C. Martin, *Appl. Phys. Lett.* **99**, 172903 (2011).
 [9] S.-W. Cheong and M. Mostovoy, *Nat. Mater.* **6**, 13 (2007).
 [10] V. Caignaert, V. Pralong, V. Hardy, C. Ritter, and B. Raveau, *Phys. Rev. B* **81**, 094417 (2010).
 [11] B. A. Frandsen, E. S. Bozin, E. Aza, A. F. Martínez, M. Feyngenson, K. Page, and A. Lappas, *Phys. Rev. B* **101**, 024423 (2020).
 [12] B. A. Trump, S. M. Koohpayeh, K. J. T. Livi, J. -J. Wen, K. E. Arpino, Q. M. Ramasse, R. Brydson, M. Feyngenson, H. Takeda, M. Takigawa, K. Kimura, S. Nakatsuji, C. L. Broholm, and T. M. McQueen, *Nat. Commun.* **9**, 2619 (2018).
 [13] F. Ye, S. Chi, H. Cao, B. C. Chakoumakos, J. A. Fernandez-Baca, R. Custelcean, T. F. Qi, O. B. Kometa, and G. Cao, *Phys. Rev. B* **85**, 180403(R) (2012).
 [14] M. A. Tovar-Olvera, P. Ruiz-Diaz, and M. Saubanere, *Phys. Rev. B* **105**, 094413 (2022).
 [15] V. Kocsis, S. Bordacs, D. Varjas, K. Penc, A. Abouelsayed, C. A. Kuntscher, K. Ohgushi, Y. Tokura, and I. Kézsmárk, *Phys. Rev. B* **87**, 064416 (2013).

- [16] J. Ma, V. O. Garlea, A. Rondinone, A. A. Aczel, S. Calder, C. dela Cruz, R. Sinclair, W. Tian, S. Chi, A. Kiswandhi, J. S. Brooks, H. D. Zhou, and M. Matsuda, *Phys. Rev. B* **89**, 134106 (2014).
- [17] M. R. Suchomel, D. P. Shoemaker, L. Ribaud, M. C. Kemei, and R. Seshadri, *Phys. Rev. B* **86**, 054406 (2012).
- [18] G. Giovannetti, A. Stroppa, S. Picozzi, D. Baldomir, V. Pardo, S. Blanco-Canosa, F. Rivadulla, S. Jodlauk, D. Nierman, J. Rohrkamp, T. Lorentz, S. Streltsov, D. I. Khomskii and J. Hemberger, *Phys. Rev. B* **83**, 060402(R) (2011).
- [19] A. Rahaman, M. Chakraborty, T. Paramanik, R. K. Maurya, S. Mahana, R. Bindu, D. Topwal, P. Mahadevan, and D. Choudhury, *Phys. Rev. B* **100**, 115162 (2019).
- [20] H. D. Zhou, J. Lu, and C. R. Wiebe, *Phys. Rev. B* **76**, 174403 (2007).
- [21] S. H. Lee, C. Broholm, T. H. Kim, W. Ratcliff II, and S. W. Cheong, *Phys. Rev. Lett.* **84**, 3718 (2000).
- [22] J.-H. Chung, S. Park, H. Ueda, Y. Ueda and S.-H. Leel, *J. Korean Phys. Soc.* **62**, 1900 (2013).
- [23] M. C. Kemei, P. T. Barton, S. L. Moffitt, M. W. Gaultois, J. A. Kurzman, Ram. Seshadri, M. R. Suchomel, and Young-il Kim, *J. Phys.: Condens. Matter* **25**, 326001 (2013).
- [24] L. Ortega-San-Martin, A. J. Williams, C. D. Gordon, S. Klemme, and J. P. Attfield, *J. Phys.: Condens. Matter* **20**, 104238 (2008).
- [25] K. Dey, S. Majumder, and S. Giri, *Phys. Rev. B* **90**, 184424 (2014).
- [26] G. T. Lin, Y. Q. Wang, X. Luo, J. Ma, H. L. Zhuang, D. Qian, L. H. Yin, F. C. Chen, J. Yan, R. R. Zhang, S. L. Zhang, W. Tong, W. H. Song, P. Tong, X. B. Zhu, and Y. P. Sun, *Phys. Rev. B* **97**, 064405 (2018).
- [27] T. A. Kaplan, *Phys. Rev.* **116**, 888 (1959).
- [28] T. A. Kaplan, *Phys. Rev.* **119**, 1460 (1960).
- [29] D. H. Lyons, T. A. Kaplan, K. Dwight, and N. Menyuk, *Phys. Rev.* **126**, 540 (1962).
- [30] N. Menyuk, K. Dwight, D. H. Lyons, and T. A. Kaplan, *Phys. Rev.* **127**, 1983 (1962).
- [31] K. Tomiyasu, J. Fukunaga, and H. Suzuki, *Phys. Rev. B* **70**, 214434 (2004).
- [32] J. M. Hastings and L. M. Corliss, *Phys. Rev.* **126**, 556 (1962).
- [33] C. Thessieu, C. Pfeleiderer, A. N. Stepanov, and J. Flouquet, *J. Phys.: Condens. Matter* **9**, 6677 (1997).
- [34] N. J. Ghimire, M. A. McGuire, D. S. Parker, B. C. Sales, J. Q. Yan, V. Keppens, M. Koehler R. M. Latture, and D. Mandrus, *Phys. Rev. B* **85**, 224405 (2012).
- [35] N. O. Golosova, D. P. Kozlenko, S. E. Kichanov, E. V. Lukin, H. P. Liermann, K. V. Glazyrin, and B. N. Savenko, *J. Alloys Compd.* **722**, 593 (2017).
- [36] P. C. Hohenberg and B. I. Halperin, *Rev. Mod. Phys.* **49**, 435 (1977).
- [37] D. Choudhury, P. Mandal, R. Mathieu, A. Hazarika, S. Rajan, A. Sundaresan, U. V. Waghmare, R. Knut, O. Karis, P. Nordblad, and D. D. Sarma, *Phys. Rev. Lett.* **108**, 127201 (2012).
- [38] Rahul Kumar, Premakumar Yanda, and A. Sundaresan, *Phys. Rev. B* **103**, 214427 (2021).
- [39] K. Vijayanandhini, Ch. Simon, V. Pralong, V. Caignaert, and B. Raveau, *Phys. Rev. B* **79**, 224407 (2009).
- [40] R. Mathieu, M. Hudl, and P. Nordblad, *Europhys. Lett.* **90**, 67003 (2010).
- [41] P. -Z. Wong, S. von Molnar, T. T. M. Palstra, J. A. Mydosh, H. Yoshizawa, S. M. Shapiro, and A. Ito, *Phys. Rev. Lett.* **55**, 2043 (1985).
- [42] H. Yoshizawa, S. Mitsuda, H. Aruga, and A. Ito, *Phys. Rev. Lett.* **59**, 2364 (1987).
- [43] G. Lawes, B. Melot, K. Page, C. Ederer, M. A. Hayward, T. Proffen, and R. Seshadri, *Phys. Rev. B* **74**, 024413 (2006).
- [44] M. C. Kemei, S. L. Moffitt, L. E. Darago, R. Seshadri M. R. Suchomel, D. P. Shoemaker, K. Page, and J. Siewenie, *Phys. Rev. B* **89**, 174410 (2014).
- [45] R. K. Maurya, N. Singh, S. K. Pandey, and R. Bindu, *Europhys. Lett.* **110**, 27007 (2015).
- [46] P. Pal, A. Rahaman, J. Brar, R. Bindu, and D. Choudhury, *J. Appl. Phys.* **132**, 183905 (2022).
- [47] C. Ederer and M. Komelj, *Phys. Rev. B* **76**, 064409 (2007).
- [48] T. Arima, Y. Watanabe, K. Taniguchi, M. Watanabe, and Y. Noda, *J. Magn. Magn. Mater.* **310**, 807 (2007).